AD-A135 483 A PLANE WAVE EXPANSION SOLUTION FOR THE SCATTERING FROM 1/1
A FREQUENCY-SELEC..(U) ROYAL SIGNALS AND RADAR
ESTABLISHMENT MALVERN (ENGLAND) J G GALLAGHER ET AL.
UNCLASSIFIED AUG 83 RSRE-MEMO-3618 DRIC-BR-89584 F/G 9/5 NL

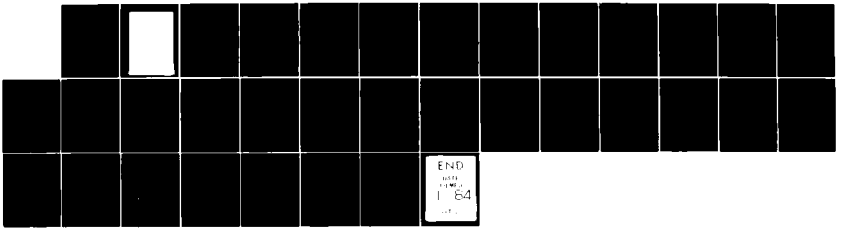

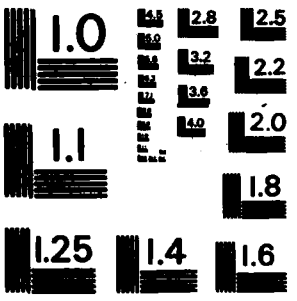

MICROCOPY RESOLUTION TEST CHART
NATIONAL BUREAU OF STANDARDS-1963-A

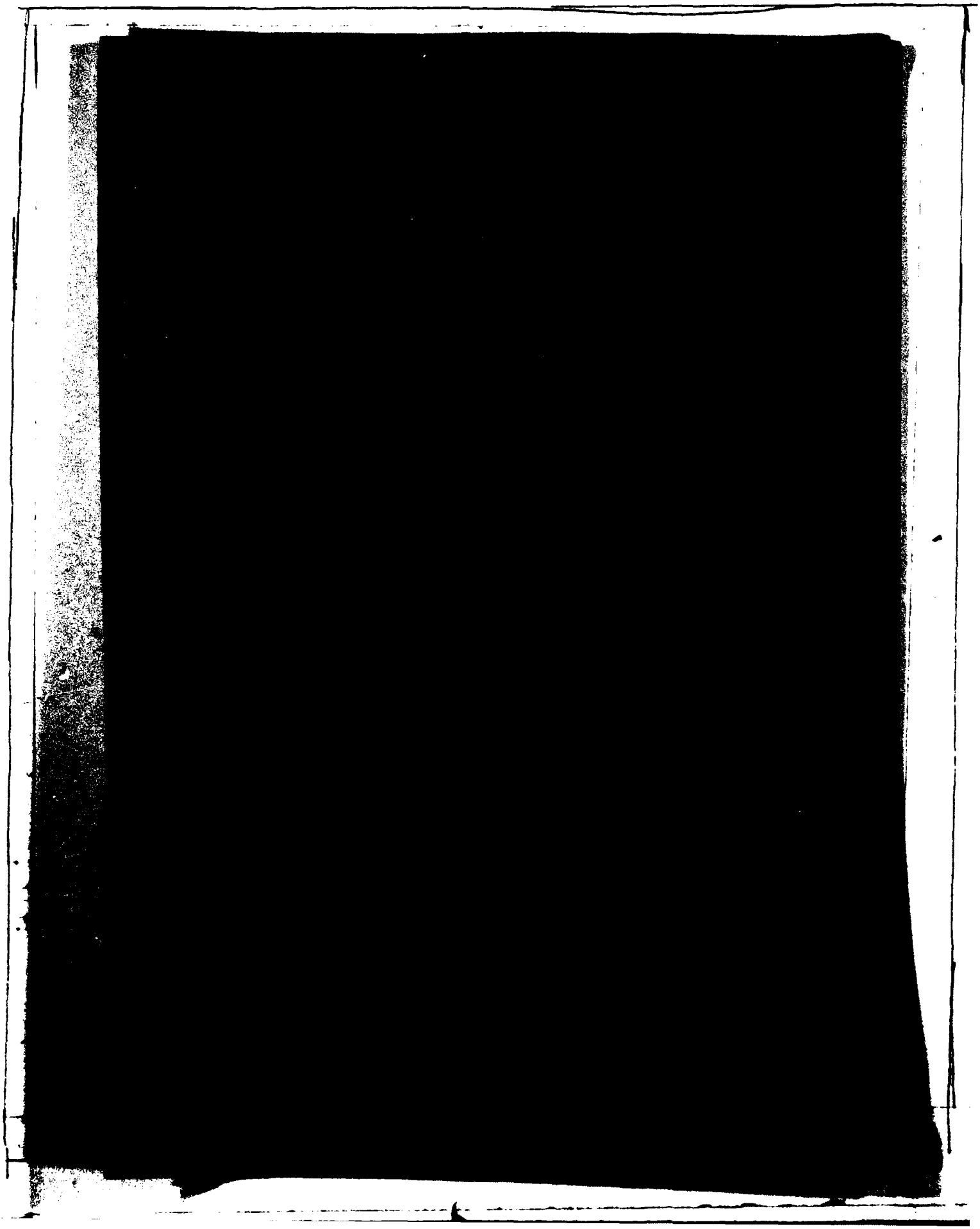

UNLIMITED

ROYAL SIGNALS AND RADAR ESTABLISHMENT

Memorandum 3618

Title: A PLANE WAVE EXPANSION SOLUTION FOR THE SCATTERING FROM A FREQUENCY-SELECTIVE SURFACE IN THE PRESENCE OF A DIELECTRIC

Authors: J G Gallagher and D J Brammer

Date: August 1983

SUMMARY

The scattering of a plane wave from a periodic broken-wire grid buried in a dielectric sheet is studied for a general angle of incidence and for arbitrary linear polarisation. The scattered field is expanded in a set of Floquet modes, and the modal coefficients are obtained through the current expansion for a reflecting antenna. The general formulation of the problem is applicable for grids in an infinite dielectric and when located at the boundary interface of two dielectrics. A moment method is used to determine the current on the grid elements and numerical results for the transmission characteristics of several different grid configurations are presented. In addition, the effect on the resonant frequency of parametric variations in the grid geometry is determined. Predicted results are compared with measured transmission characteristics and show excellent agreement.

INTRODUCTION

The use of dichroic or frequency selective surfaces in a wide variety of applications has attracted a lot of attention in recent years [Agrawal and Imbriale, 1979; Arnaud and Pelow, 1975; Munro et al, 1981; Pedersen and Hannan, 1982]. These structures are, in general, comprised of a periodic array of metallic patches printed on a dielectric substrate, or of periodic apertures in a conducting screen. Volume and weight constraints imposed by satellite system launch vehicles require that a satellite antenna be capable of multi-frequency band operation and the use of frequency selective surfaces in either the main reflector or the sub-reflector has the potential for meeting this requirement. Another important application is in the area of antenna spatial filtering, which allows an incident wave to pass if it is within the filter's angular passband and rejects those waves that are incident at an angle outside the passband.

Our interest in the reactive surface has stemmed from a need to increase our radome design flexibility. The dielectric walls of radomes can be successfully matched to free space by incorporating reactive surfaces in the radome build. A well established matching technique, which gives an extra degree of freedom in the design of both solid and sandwich radomes, is the use of continuous wires oriented so that the electric vector of the incident wave is parallel to the wires. Continuous wire grids can be used to reduce radome aberration, and also have application in the design of dual-frequency antennas. There are, however, other structures with transmission and reflection properties, which vary with frequency, that are potentially more versatile in their application to multi-band systems.

Agrawal and Imbriale [1979], described the use of crossed dipoles in the design of a Cassegrain subreflector for a dual-frequency reflector antenna. Pelton and Munk [1974], have studied the transmission characteristics of a metallic radome having a resonant slotted periodic surface. A D-band antenna design using a printed rectangular metallic grid within a dielectric was reported by Cary [1977]. The size and pitch of the grid was chosen so that the structure was transparent to I-band, thus enabling D-band and I-band antennas to be located in the same aperture with a negligible degradation of the I-band performance.

In this paper we describe a theoretical investigation into the transmission characteristics of a resonant periodic grid of broken wires, which behaves as a capacitive structure below resonance and inductive above resonance. We shall present a general formulation of the scattering problem that can apply whether the grid is in an infinite dielectric, or on the surface of a dielectric sheet, or buried in a dielectric sheet, and we shall compare measured results with our theoretical predictions. Several workers have tackled the problem of scattering by a two-dimensional periodic array of rectangular conducting plates. Ott et al [1967], used a point-matching technique to investigate the scattering of a normally incident plane wave from such an array when arranged in a rectangular lattice in free space. Chen [1970], used the method of moments to solve the problem for arbitrary incidence angle on a skew-periodic array, and Montgomery [1975], extended this work to account for the effects of the dielectric when the array of conductors is supported on a dielectric substrate.

The procedure to be presented here is to determine the transmission and reflection characteristics of an infinite broken-wire grid buried in a

dielectric sheet through the expansion of the electromagnetic field in an infinite spectrum of plane waves. The two-dimensional periodicity of the grid enables the scattered field to be expanded in a set of Floquet modes, which are solutions to the wave equation satisfying the appropriate periodicity. These Floquet modes undergo multiple reflections at the dielectric boundary interfaces, and using superposition the field in the presence of the dielectric can be determined. The Floquet mode coefficients are obtained using the current expansion for a reflecting antenna, and the scattered field is determined by summing the Floquet modes at the appropriate observation point. A moment method [Thiele, 1973], is used to determine the current expansion, invoking a form of the thin wire approximation. The boundary condition of zero electric field along the wire is enforced by Galerkin testing, thus ensuring a stationary solution for the current. From the current distribution determined on the wires the scattered field is calculated, which when added to the incident field yields the total transmitted and reflected fields.

THEORY

Consider the geometry shown in Fig 1 for an infinite planar array of cylindrical wires arranged periodically along skewed co-ordinates η_1 and η_2. The wires are assumed identical with a wire radius a, and length ℓ, and are buried in a dielectric sheet of permittivity ϵ_2. A linearly polarised plane wave is incident on the grid-dielectric structure at an angle (θ,ϕ) and the periodicity of the grid allows the scattered field to be expanded in a set of Floquet modes [Amitay et al., 1972],

$$\psi_{mn} = A_{mn} \exp(-j(k_{xm}x + k_{yn}y + \Gamma_{mn}z)) \qquad (1)$$

where

$$k_{xm} = kt_x + \frac{2\pi m}{b} \tag{2}$$

$$k_{yn} = kt_y + \frac{2\pi n}{c} + \frac{2\pi m}{b\tan\gamma} \tag{3}$$

$$\varepsilon_r k_1^2 = k_{xm}^2 + k_{yn}^2 + \Gamma_{mn}^2, \quad m,n = 0, \pm 1, \pm 2, \ldots \tag{4}$$

and t_x, t_y, t_z are the direction cosines of the wave incident on the dielectric sheet and k_1 is its wavenumber, $\varepsilon_r = \varepsilon_2/\varepsilon_1$

The modal propagation constant, Γ_{mn}, is either real or imaginary and depends on the mode order, (ie the m,n values). The array spacing and angle of incidence determine the number of propagating modes, which exist for real Γ_{mn}. A complete set of orthonormalised vector TE and TM Floquet modes can be derived from the scalar wave function, ψ_{mn}. The orthonormalised vector mode for the TE case is,

$$\underset{\sim}{\psi}_{1mn} = (bc)^{-\frac{1}{2}} \frac{(-k_{yn}\hat{x} + k_{xm}\hat{y})}{(\varepsilon_r k_1^2 - \Gamma_{mn}^2)^{\frac{1}{2}}} \exp(-j(k_{xm}x + k_{yn}y)), \tag{5}$$

and the modal admittance is,

$$Y_{1mn} = \frac{\Gamma_{mn}}{\omega\mu}, \tag{6}$$

Similarly, the orthonormalised TM vector mode is,

$$\underset{\sim}{\psi}_{2mn} = (bc)^{-\frac{1}{2}} \frac{(k_{xm}\hat{x} + k_{yn}\hat{y})}{(\varepsilon_r k_1^2 - \Gamma_{mn}^2)^{\frac{1}{2}}} \exp(-j(k_{xm}x + k_{yn}y)), \tag{7}$$

and the modal admittance is,

$$Y_{2mn} = \frac{\omega\varepsilon_2}{\Gamma_{mn}}, \tag{8}$$

A general solution for the field from the grid of broken wires is given by,

$$\underset{\sim}{E} = \sum_{p}\sum_{q} A_{pq} \exp(-j(k_{xp}x+k_{yq}y+\Gamma_{pq}z)) \frac{(\hat{s}(\hat{s}.\hat{x})-\hat{x})}{(1-(\hat{s}.\hat{x})^2)^{\frac{1}{2}}} \tag{9}$$

$$\underset{\sim}{H} = (\epsilon_2/\mu)^{\frac{1}{2}} \hat{s}x\underset{\sim}{E} , \tag{10}$$

where $\hat{s}$ is the wave normal unit vector and μ is the permeability of the dielectric.

The coefficient A_{pq}, in (9), can be determined by applying Amperes theorem to a small element on the current plane and by using orthogonality and integrating over a periodic unit cell. The result is,

$$A_{p'q'} = \frac{(\mu/\epsilon_2)^{\frac{1}{2}}}{2bc} \frac{(1-(\hat{s}.\hat{x}))^{\frac{1}{2}}}{|\hat{s}.\hat{z}|} \int_{\ell/2}^{\ell/2} I(x)\exp(jk_{xp'}x)dx, \tag{11}$$

To determine the field inside the dielectric sheet we resolve the field from the incident plane wave into components perpendicular and parallel to the plane of incidence. Thus a plane wave incident from medium 1 ($z < 0$) onto the plane $Z = 0$ can be expressed as,

$$\underset{\sim}{E}(\underset{\sim}{r}) = \underset{\sim}{E}_o \exp(-jk_1 \hat{t}_1 . \underset{\sim}{r}) , \tag{12}$$

and in terms of perpendicular and parallel incidence,

$$\underset{\sim}{E}(r) = (\underset{\sim}{E}^{\perp} + \underset{\sim}{E}^{\parallel}_o) \exp(-jk_1 \hat{t}_1 . \underset{\sim}{r}) , \tag{13}$$

where the perpendicular component is,

$$\underset{\sim}{E}^{\perp}_o = (\hat{z}x\hat{t}_1 . \underset{\sim}{E}_o) \frac{\hat{z}x\hat{t}_1}{|\hat{z}x\hat{t}_1|^2} , \tag{14}$$

and the parallel component is,

$$\underset{\sim}{E}^{\parallel}_o = E_z \frac{(\hat{z} - (\hat{t}_1.\hat{z})\hat{t}_1)}{1 - (\hat{t}_1.\hat{z})^2} , \tag{15}$$

$\hat{t}_1$ is the unit vector wave normal of the incident plane wave which has arbitrary linear polarisation $\underset{\sim}{E}_o = E_x\hat{x} + E_y\hat{y} + E_z\hat{z}$. The field inside the slab at an arbitrary position ($z=d_2+a$, say) is obtained by a superposition of right-travelling and left-travelling plane waves arising from multiple reflections at the dielectric boundary interfaces Z=0, and $z=d_1+d_2$. The general expression for the field inside the dielectric is, therefore, given by,

$$\underset{\sim}{E}_D = \underset{\sim}{E}_D^{\perp} + \underset{\sim}{E}_D^{\parallel} , \tag{16}$$

where, for the perpendicular incidence component,

$$\underset{\sim}{E}_D^{\perp} = (\hat{z}\times\hat{t}_1.\underset{\sim}{E}_o)\frac{\hat{z}\times\hat{t}_1}{|\hat{z}\times\hat{t}_1|^2} T_{12}^{\perp} \frac{\exp(-jk_2t_{2z}d_2)}{1-M_1^{\perp}M_2^{\perp}}$$

$$.(\exp(-jk_2t_{2z}a) + M_1^{\perp}\exp(jk_2t_{2z}a)) , \tag{17}$$

and for the parallel incident component

$$\underset{\sim}{E}_D^{\parallel} = \frac{k_1}{k_2}\frac{E_z}{(1-(\hat{t}_1.\hat{z})^2)}\frac{T_{12}^{\parallel}\exp(-jk_2t_{2z}d_2)}{1-M_1^{\parallel}M_2^{\parallel}}\Big(-t_{2z}(t_{1x}\hat{x}+t_{1y}\hat{y})(\exp(-jk_2t_{2z}a)$$

$$-M_1^{\parallel}\exp(jk_2t_{2z}a)) + \hat{z}(1-(\hat{t}_1.\hat{z})^2(\varepsilon_1/\varepsilon_2)^{\frac{1}{2}}(\exp(-jk_2t_{2z}a) \tag{18}$$

$$+M_1^{\parallel}\exp(jk_2t_{2z}))\Big)$$

where,

$$M_1^{\perp} = R_{21}^{\perp}\exp(-j2k_2t_{2z}d_1)$$

$$M_2^{\perp} = R_{21}^{\perp}\exp(-j2k_2t_{2z}d_2)$$

$$R_{21}^{\perp} = \frac{\epsilon_2^{\frac{1}{2}}\,\hat{t}_2\cdot\hat{z} - \epsilon_1^{\frac{1}{2}}\,\hat{t}_1\cdot\hat{z}}{\epsilon_2^{\frac{1}{2}}\,\hat{t}_2\cdot\hat{z} + \epsilon_1^{\frac{1}{2}}\,\hat{t}_1\cdot\hat{z}}$$

$$T_{12}^{\perp} = \frac{2\epsilon_1^{\frac{1}{2}}\,\hat{t}_1\cdot\hat{z}}{\epsilon_2^{\frac{1}{2}}\hat{t}_2\cdot\hat{z} + \epsilon_1^{\frac{1}{2}}\hat{t}_1\cdot\hat{z}}$$

$$M_1^{\parallel} = R_{21}^{\parallel}\exp(-j2k_2t_{2z}d_1)$$

$$M_2^{\parallel} = R_{21}^{\parallel}\exp(-j2k_2t_{2z}d_2)$$

$$R_{21}^{\parallel} = \frac{\epsilon_1^{\frac{1}{2}}\hat{t}_2\cdot\hat{z} - \epsilon_2^{\frac{1}{2}}\hat{t}_1\cdot\hat{z}}{\epsilon_1^{\frac{1}{2}}\hat{t}_2\cdot\hat{z} + \epsilon_2^{\frac{1}{2}}\hat{t}_1\cdot\hat{z}}$$

$$T_{12}^{\parallel} = \frac{2\,\epsilon_2^{\frac{1}{2}}\,\hat{t}_1\cdot\hat{z}}{\epsilon_1^{\frac{1}{2}}\hat{t}_2\cdot\hat{z} + \epsilon_2^{\frac{1}{2}}\,\hat{t}_1\cdot\hat{z}}$$

We now obtain an expression for the field from the grid at the wire surface by summing the Floquet modes following reflection at the boundary interfaces, $z = 0$ and $z = d_1+d_2$. The Floquet modes scattered to the right of the wire grid plane, $z = d_2$, and those scattered to the left can be resolved into right-travelling and left-travelling waves. The superposition of these waves at the wire surface ($z = d_2+a$), in terms of their TE and TM components, gives the expression for the field at the wire surface resulting from the Floquet mode expansion. Thus, the fields can be written,

$$\underline{E}_{1F} = \frac{(\mu/\epsilon_2)^{\frac{1}{2}}}{2bc}\sum_p\sum_q \frac{(\hat{s}\cdot\hat{y})}{|\hat{s}\cdot\hat{x}|}\,\frac{\hat{z}\times\hat{s}}{|\hat{z}\times\hat{s}|}\int_{-\frac{b}{2}}^{\frac{b}{2}} I(x)\exp(jk_{xp}x)dx$$

$$\frac{(1+N_2^{\perp})}{(1-N_1^{\perp}N_2^{\perp})} \left(\exp(-j\Gamma_{pq}a) + N_1^{\perp} \exp(j\Gamma_{pq}a)\right) , \tag{19}$$

$$\underset{\sim}{E}_{2F} = \frac{(\mu/\varepsilon_2)^{\frac{1}{2}}}{2bc} \sum_p \sum_q \frac{(\hat{s}.\hat{x})}{|\hat{z}x\hat{s}|^2} \int_{-\frac{L}{2}}^{\frac{L}{2}} I(x) \exp(jk_{xp}x)dx \tag{20}$$

$$\frac{(1+N_2^{\parallel})}{(1-N_1^{\parallel}N_2^{\parallel})} \left(\hat{s}x(\hat{z}x\hat{s})\exp(-j\Gamma_{pq}a) - (\hat{s}(\hat{s}.\hat{z})+\hat{z}(1-2(\hat{s}.\hat{z})^2)N_1^{\parallel} \exp(j\Gamma_{pq}a)\right),$$

where $\underset{\sim}{E}_{1F}$ is the field resulting from the TE Floquet modes, and $\underset{\sim}{E}_{2F}$ is the field from the TM Floquet modes.

$$N_1^{\parallel} = \rho_{21}^{\parallel} \exp(-j2(\hat{s}.\hat{z})d_1)$$

$$N_2^{\parallel} = \rho_{21}^{\parallel} \exp(-j2(\hat{s}.\hat{z})d_2)$$

$$N_1^{\perp} = \rho_{21}^{\perp} \exp(-j2(\hat{s}.\hat{z})d_1)$$

$$N_2^{\perp} = \rho_{21}^{\perp} \exp(-j2(\hat{s}.\hat{z})d_2)$$

The reflection coefficients, $\rho_{21}^{\perp}$ and $\rho_{21}^{\parallel}$ can be specified through the modal admittances, Y_{1pq} and Y_{2pq} respectively.

$$\rho_{21}^{\perp} = \frac{Y_{1pq}^{(2)} - Y_{1pq}^{(1)}}{Y_{1pq}^{(2)} + Y_{1pq}^{(1)}} , \tag{21}$$

$$\rho_{21}^{\parallel} = \frac{Y_{2pq}^{(2)} - Y_{2pq}^{(1)}}{Y_{2pq}^{(2)} + Y_{2pq}^{(1)}} , \tag{22}$$

The superscripts, (1) and (2), on the modal admittances refer to media 1 and 2 respectively.

The scattered field in the forward direction, $z > d_1 + d_2$, can be determined from the forward-travelling wave expressions in equations (19) and (20), and by applying the boundary conditions at the interface, $z=d_1+d_2$. Thus, the forward scattered fields are given by,

$$\underset{\sim}{E}_{1sf} = \frac{(\mu/\epsilon_2)^{\frac{1}{2}}}{bc} \sum_p \sum_q \frac{\hat{s}.\hat{y}}{|\hat{s}.\hat{z}|} \frac{\hat{z}x\hat{s}}{|\hat{z}x\hat{s}|^2} \frac{(1+N_2^{\perp})}{(1-N_1^{\perp}N_2^{\perp})} \frac{\epsilon_2^{\frac{1}{2}}(\hat{s}.\hat{z})}{(\epsilon_1^{\frac{1}{2}}(\hat{s}_1.\hat{z})+\epsilon_2^{\frac{1}{2}}(\hat{s}.\hat{z}))}$$

$$\exp(-j\Gamma_{pq}d_1) \cdot \int_{-\frac{\ell}{2}}^{\frac{\ell}{2}} I(x) \exp(jk_{xp}x)dx \ , \qquad (23)$$

$$\underset{\sim}{E}_{2sf} = \frac{(\mu/\epsilon_1)^{\frac{1}{2}}}{bc} \sum_p \sum_q \frac{(\hat{s}.\hat{x})}{|\hat{z}x\hat{s}|^2} (\hat{s}x\hat{z})x\hat{s}_1 \frac{(1+N_2^{\parallel})}{(1-N_1^{\parallel}N_2^{\parallel})} \frac{\epsilon_1^{\frac{1}{2}}(\hat{s}.\hat{z})}{(\epsilon_1^{\frac{1}{2}}(\hat{s}.\hat{z})+\epsilon_2^{\frac{1}{2}}(\hat{s}_1.\hat{z}))}$$

$$\exp(-j\Gamma_{pq}d_1) \cdot \int_{-\frac{\ell}{2}}^{\frac{\ell}{2}} I(x)\exp(jk_{xp}x)dx \qquad (24)$$

Similarly, the scattered field in the backward direction, $z<0$, can be determined from the backward-travelling wave expressions. The backward scattered fields are

$$\underset{\sim}{E}_{1sb} = \frac{(\mu/\epsilon_2)^{\frac{1}{2}}}{bc} \sum_p \sum_q \frac{\hat{s}.\hat{y}}{|\hat{s}.\hat{z}|} \frac{\hat{z}x\hat{s}}{|\hat{z}x\hat{s}|^2} \frac{(1+N_1^{\perp})}{(1-N_1^{\perp}N_2^{\perp})} \frac{\epsilon_2^{\frac{1}{2}}(\hat{s}.\hat{z})}{(\epsilon_1^{\frac{1}{2}}(\hat{s}_1.\hat{z})+\epsilon_2^{\frac{1}{2}}(\hat{s}.\hat{z}))}$$

$$\exp(-j\Gamma_{pq}d_2) \cdot \int_{-\frac{\ell}{2}}^{\frac{\ell}{2}} I(x)\exp(jk_{xp}x)dx \qquad (25)$$

$$\underset{\sim}{E}_{2sb} = -\frac{(\mu/\epsilon_1)^{\frac{1}{2}}}{bc}\sum_p\sum_q \frac{(\hat{s}.\hat{x})}{|\hat{z}x\hat{s}|^2}(\hat{s}x\hat{z}) \times \hat{s}_1 \frac{(1+N_1^{\parallel})}{(1-N_1^{\parallel}N_2^{\parallel})} \frac{\epsilon_1^{\frac{1}{2}}(\hat{s}.\hat{z})}{(\epsilon_1^{\frac{1}{2}}(\hat{s}.\hat{z}) + \epsilon_2^{\frac{1}{2}}(\hat{s}.\hat{z}))}$$

$$\cdot \exp(-j\Gamma_{pq}d_2)\int_{-\frac{\ell}{2}}^{\frac{\ell}{2}} I(x)\exp(jk_{xp}x)dx, \qquad (26)$$

where $\hat{s}_1$ is the unit vector wavenormal in medium 1.

We have, therefore, obtained expressions for the forward and backward scattered fields and the moment method can now be used to determine the current on the wire elements. A form of thin wire approximation is used where the incident and scattered fields are averaged over the wire surface. In general when using moment methods there are an infinite number of basis functions and weighting functions that can be used to solve the integral equation. For this particular problem accurate results are obtained by using Galerkin's method with a single basis function and a single testing function. The basis function used is the asymptotic current distribution on a reflecting antenna [Schelkunoff and Friis, 1952],

$$I(x) = \frac{\cos(k\ell/2)\cos(\hat{r}.\hat{x}\ kx) - \cos(\hat{r}.\hat{x}\ k\ell/2)\cos(kx)}{\cos(k\ell/2) - \cos(\hat{r}.\hat{x}\ k\ell/2)}, \qquad (27)$$

where $\hat{r}$ is the unit vector wavenormal of the wave incident on the wire antenna. The advantage in using this basis function is that it leads to efficient computation and that the integral in the field expressions can be evaluated analytically. Thus,

$$\int_{-\frac{\ell}{2}}^{\frac{\ell}{2}} I(x)\exp(jk_{xp}x)dx = \frac{2\cos(k\ell/2)\cos(\hat{r}.\hat{x}k\ell/2)\cos(k_{xp}\ell/2)}{\cos(k\ell/2) - \cos(\hat{r}.\hat{x}\ k\ell/2)}$$

$$\left(\frac{(\hat{r}.\hat{x}\ k\ \tan(\hat{r}.\hat{x}k\ell/2) - k_{xp}\tan(k_{xp}\ell/2))}{((\hat{r}.\hat{x})^2k^2-k_{xp}^2)} - \frac{(k\tan(k\ell/2)-k_{xp}\tan(k_{xp}\ell/2))}{(k^2-k_{xp}^2)}\right) \quad (28)$$

When the currents on the grid have been calculated the scattered field from these currents is added to the field transmitted through the dielectric sheet in the absence of the wire grid to give the transmitted far field. Similarly the reflected field is the superposition of the backward scattered field and the field reflected from the dielectric sheet without the presence of the grid.

As the dielectric sheet becomes very thin, this is comparable with a few wire parameters, the form of the current distribution tends to that of the wires in free space. To emphasise this the I(X) of (27) can be written as,

$$I(x) = \alpha I\ (k_1, x)\ 4\ \beta I\ (k_2, x) \quad (29)$$

where $I(k_1, x)$ is the current on the wires in free space, $I(k_2, x)$ is the current on the wires in an infinite dielectric and where k_2 is the wavenumber for the dielectric, and k_1, is the free space wavenumber. For thin dielectric sheets these two functions are used as the two basis functions in the moment method calculation in order to prevent an unreal current distribution being forced on the problem and giving erroneous results. Galerkin's method is used whereby the same two functions are used for testing so that it becomes necessary to solve two equations to obtain α and β. This procedure has been found to be necessary for thin sheets of dielectric and is also applicable when the wire-grid is at the surface

of the dielectric sheet. It can, of course, be used for all calculations since the penalty in computation time is minimal.

EXPERIMENTAL METHOD AND MEASUREMENTS

The experimental frequency selective surfaces of periodically broken wires, having a skew angle, γ, of 41° were constructed by printing the copper elements on a flexible polyimide film using standard photolithographic techniques. The individual wire elements were 15mm long, with their centres on a triangular lattice, their lateral spacing (pitch) 7.5mm, and their longitudinal spacing 17.5mm. Two sheets of polyimide were used to sandwich the grid in the centre of the dielectric sheet to give a dielectric thickness of 0.42mm. To ensure a rigid planar configuration the grid arrays were mounted between sheets of polystyrene foam, which had little effect on the measured properties. Measurements of the phase and amplitude of waves transmitted through a large plane sheet of the grid were made for angles of incidence from 0° to 50° for perpendicular polarisation.

The transmission characteristics of the grid were measured in the frequency range 8-12GHz using the free-space bridge arrangement shown in Fig 2. The incident field was polarised parallel to the grid wires, and to ensure plane wave conditions the set-up was designed so that the grid was in the far-field of the illuminating and receiving antennas. The physical area of the grid was much larger than the illuminated area, so it can be regarded as effectively infinite in extent. At the higher angles of incidence, however, this assumption breaks down and edge effects cause variations in the transmission properties of the grid at angles of 70° and above. For angles of incidence up to 50° the main experimental difficulty was the large dynamic range of the transmitted test signals. The experimental errors are estimated to be not more than $\pm 5^{\circ}$ in phase and $\pm$ 0.5dB in amplitude.

Initial measurements of the transmission properties of broken-wire grids were carried out with the grids on the dielectric surface and these results showed a transition from capacitive to inductive behaviour as the frequency increases through resonance. This type of response was typical for all the grids that were measured. There is a marked shift in the resonance frequency when the grid is printed on dielectric substrates of different thicknesses. For instance, the resonant frequency increases by more than 6% when the substrate thickness changes from 0.15 mm to 0.05 mm.

A number of broken-wire grids were manufactured with different dipole lengths, wire pitches and printed on substrates of different thicknesses. All the grids measured exhibited one common feature, namely that each grid behaved like a series RLC circuit shunted across a free-space transmission line. The experimental results presented in this paper, however, will only be for the grid with fixed dimensions listed above and located at the centre of a polyimide sheet 0.42mm thickness with a relative permittivity $\epsilon_r = 4.2$.

Figures 3, 4 and 5 show the transmission response in phase and amplitude for incidence angles of 0°, 20° and 50°. The resonance frequency, 8.47 GHz, remains constant with increasing incidence angle, and the loss curves are almost identical. At 50° incidence there is a definite broadening of the loss curve and the phase response overshoots the $\pm 90^\circ$ values when switching from positive to negative phase as the frequency goes through resonance. This phase characteristic becomes more pronounced with increasing incidence angle and may be due, in part, to the finite nature of the grid under test. A larger grid may reduce this effect by presenting a larger projected grid area to the incident wave.

PREDICTED RESULTS

In this section we present calculated results for the transmission characteristics of several broken wire grids having different geometrical configurations. Theoretical predictions are given for grids with different skewed co-ordinate axes, where the skew angle, γ, is either 41° or 90°. The transmission properties of a periodic grid are given both in an infinite dielectric and when buried in the centre of a dielectric sheet. In addition the effect on the free-space resonant frequency is plotted for parametric variations of the grid periodicities and wire radius. Finally, we compare the predicted results with the measured results of the previous section. All the predictions are for a perpendicularly polarised wave incident on the grid such that the incident field is polarised parallel to the grid wires. The calculations, except where it is specifically stated otherwise, are for a grid geometry with 15mm long wire elements, a pitch of 7.5mm, and a longitudinal spacing of 17.5mm. All the predictions are obtained using the basis function of (27), except for the experimental grid buried in the thin dielectric sheet, which uses the current distribution of (29).

The phase and amplitude response of a grid with a skew angle of 41° is shown in Fig. 6 calculated over the frequency range 3-15 GHz for incidence angles from 0° to 80°. The grid is located in free space and exhibits a resonance at 10.8 GHz for all the angles of incidence. A notable feature in the amplitude curves is the broadening response with angle of incidence and the fixed resonant frequency. Figure 7 shows the transmission characteristics for the same free-space grid but with a skew angle of 90°. Here we see that the resonant frequency decreases with increasing incidence angle going from 11.3 GHz at 0° to 10.8 GHz at 80°. The phase response is almost identical to the 41° grid except, of course, for the cross-over resonant frequency.

Figure 8 shows the transmission response of a grid with a skew angle of 90° in an infinite dielectric of relative permittivity 4. We note that the resonant frequency has shifted down to the region around 5.5 GHz and that this frequency also decreases with increasing incidence angle. Furthermore, we observe that the transmission coefficient in the frequency neighbourhood where one of the space harmonics is diffracted at $\pm 90^{\circ}$ approaches unity. This is the well known phenomenon known as the Wood's anomaly.

When the grid is buried in a dielectric sheet the transmission characteristics for this configuration are modified by the presence of the dielectric to free-space interfaces. In particular, the resonant frequency will lie in the range bounded by the values obtained when the grid is located in free space and when the dielectric is infinite in extent. Furthermore, because the dielectric sheet is capable of sustaining bound surface waves the grid will excite these surface waves at specific frequencies when the transverse propagation constants, corresponding to the Floquet modes and to values obtained from the eigenvalue equation for an infinite dielectric sheet, are equivalent. The transmission response of a grid with a skew angle of 90° and buried in a dielectric sheet is shown in Fig 9. The sheet is 2.5 mm thick with a relative permittivity of 4 and the resonant frequency occurs in the region of 6.5 GHz. At 12.8 GHz the transmission dip in the 0° incidence curve corresponds to the excitation of the lowest order TE slab waveguide mode.

The resonant frequency of a broken-wire grid depends on the grid geometry, the dielectric constant, the thickness of the dielectric, the wire radius, and the periodicities of the grid. In Fig. 10 the resonant frequency of a wire grid in free space is plotted against the x-directed grid periodicity

normalised to the length of a wire element. The resonance is plotted for two wire radii and for parametric variations in the y-directed periodicity, which is also normalised to the wire element length. All the results are calculated for a plane wave normally incident on a grid with a skew angle of 90°. A notable feature of these curves is the relative insensitivity of the resonant frequency to variations in the normalised longitudinal periodicity. The more significant effect on the resonant frequency occurs with the change in pitch, which can vary the resonant frequency by up to 5 GHz for normalised pitches from 0.16 to 1. Another interesting feature of these results is the convergence of the curves for the 3 thou and 6 thou wire radii when the pitch is a third of the wire element length. This suggests that to maintain a relative insensitivity of the resonant frequency to parametric variations in the grid geometry then the lateral periodicity is the most important parameter to control and that it should have a value approximately one third that of the element length.

Finally, we consider the predicted results for a grid buried in a dielectric sheet with the same dielectric constant, thickness, and grid geometry as the experimental grid whose transmission characteristics are shown in Figs. 3, 4 and 5. The wire radius was obtained by taking the circumference of a printed element of the experimental grid and equating it with a cylindrical wire. The value used in the calculations was 6 thou. Since the thickness of the dielectric sheet is comparable with a few wire diameters two basis functions are used in the moment method calculation. Thus, the current distribution of (29) was used to provide accurate predictions of the transmission characteristics of the grid. Fig. 11 shows the predicted phase and amplitude response of the grid at the three angles of incidence - 0°, 20°, and 50° - using 20 p-modes and 20 q-modes for the Floquet mode expansion. The calculated resonant frequency of 8.36 GHz is

in excellent agreement with the measured value of 8.47 GHz. At the 50° incidence angle there is a clear frequency widening in the amplitude resonance curve, while the 0° and 20° curves are almost identical. These are the same features observed in the experimental measurements. Comparison of the phase curves requires further comment, namely that around resonance the experimental errors in the measurement of phase are more significant due to the lower power levels in the sampled signal. The comparison between measured and predicted phase, therefore, is more reliable away from resonance. The predicted phase response shows that at frequencies on either side of the resonance there are higher absolute phase values for the 50° incidence curve, while the 0° and 20° curves are almost identical. This same feature also exists in the measured phase curves when comparisons are made away from the resonance region.

CONCLUSIONS

We have obtained expressions for the scattering of a plane wave from a periodic grid of broken wires buried in a dielectric sheet. These expressions can also be used to predict the scattering characteristics when the grid is in an infinite dielectric and when it is at the surface of a dielectric sheet. Comparison of predicted transmission characteristics with measured results for a grid buried in a thin polyimide sheet are in excellent agreement. The approach can be simply extended to predict the scattering performance of a grid in a planar multi-layer dielectric e.g. an A-sandwich radome structure.

REFERENCES

Agrawal, V. D., and W. A. Imbriale (1979), Design of a dichroic Cassegrain subreflector, IEEE Trans Ant. and Prop., AP-27, 466-473.

Amitay, N., V Galindo, C. P. Wu (1972), Theory and Analysis of Phased Array Antennas, Wiley-Interscience, New York.

Arnaud, J.A., and F. A. Pelow (1975), Resonant-grid quasi-optical diplexers, BSTJ, 54, 263-283.

Cary, R. H. J. (1977), Some novel techniques for avoiding antenna obscurations and EMC effects, Radar 77, London, IEE Conference Publication No 155.

Chen, C-C (1970), Scattering by a two-dimensional periodic array of conducting plates, IEEE Trans. Ant. and Prop., AP-18, 660-665.

Montgomery, J. P. (1975), Scattering by an infinite periodic array of thin conductors on a dielectric sheet, IEEE Trans. Ant. and Prop., AP-23, 70-75.

Munro, A. M., G. N. Taylor, and J. G. Gallagher (1981), Inductive wire matching techniques for dual frequency microwave antennas and radomes. Proc. IVth International Conference on Electromagnetic Windows, Bandol, France.

Pedersen, J. F., and P. W. Hannan (1982), A metal-grid 5 x 5 foot angular filter, IEEE International Symp. Ant. and Prop. Vol. 2, University of New Mexico, Albuquerque.

Pelton, E. L., and B. A. Munk (1974), A streamlined metallic radome, IEEE Trans. Ant. and Prop., AP-22, 799-803.

Schelkunoff, S. A., and H. T. Friis (1952), Antennas Theory and Practice, Chapt. 8, J. Wiley, New York.

Thiele, G. A. (1973), Wire antennas, in Computer Techniques for Electromagnetics, edited by R. Mittra, Pergamon, Oxford.

Figure Captions

Fig 1 Broken-wire grid array geometry.

Fig 2 Free-space r.f. bridge; a) is the test piece, located between the transmitting horn b) and receiving horn c) and d) is a coaxial air-spaced line.

Fig 3 Measured transmission response for 0^{o} incidence.

Fig 4 Measured transmission response for 20^{o} incidence.

Fig 5 Measured transmission response for 50^{o} incidence.

Fig 6 Predicted transmission response of a free-space grid with a skew angle, γ, of 41^{o}.

Fig 7 Predicted transmission response of a free-space grid with a skew angle, γ, of 90^{o}.

Fig 8 Predicted transmission response of a broken-wire grid with a skew angle, γ, of 90^{o}, located in an infinite dielectric medium of relative permittivity 4.

Fig 9 Predicted transmission response of a broken-wire grid with a skew angle, γ, of 90^{o}, buried in the centre of a dielectric sheet 2.5mm thick and of relative permittivity 4.

Fig 10 Resonant frequency of a free-space grid with a skew angle, γ, of 90^{o} as a function of the normalised x-directed periodicity and for parametric variations of the wire radius and y-directed periodicity. All the results are predicted for a normally incident plane wave.

Fig 11 Predicted phase and amplitude response of a grid with skew angle, γ, 41^{o} and buried in the centre of a dielectric sheet 0.42 mm thick and of relative permittivity 4.2.

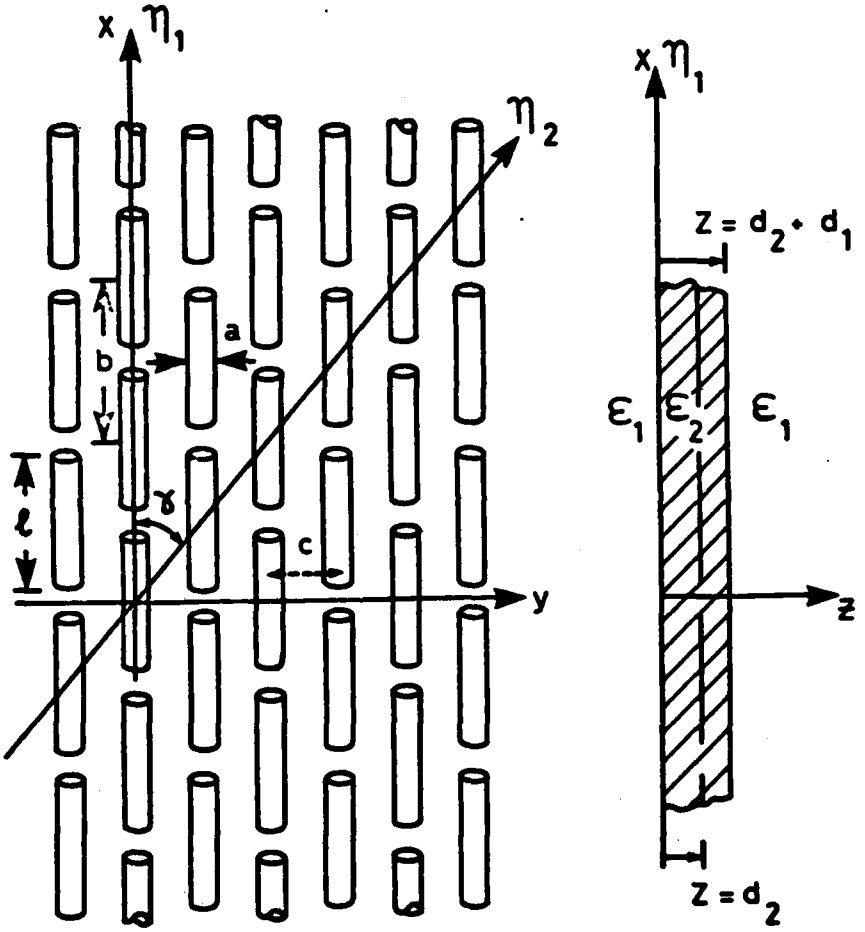
x
η_1
η_2
a
b
ℓ
γ
c
y
x
η_1
$Z = d_2 + d_1$
ε_1
ε_2
ε_1
z
$Z = d_2$

FIG 1

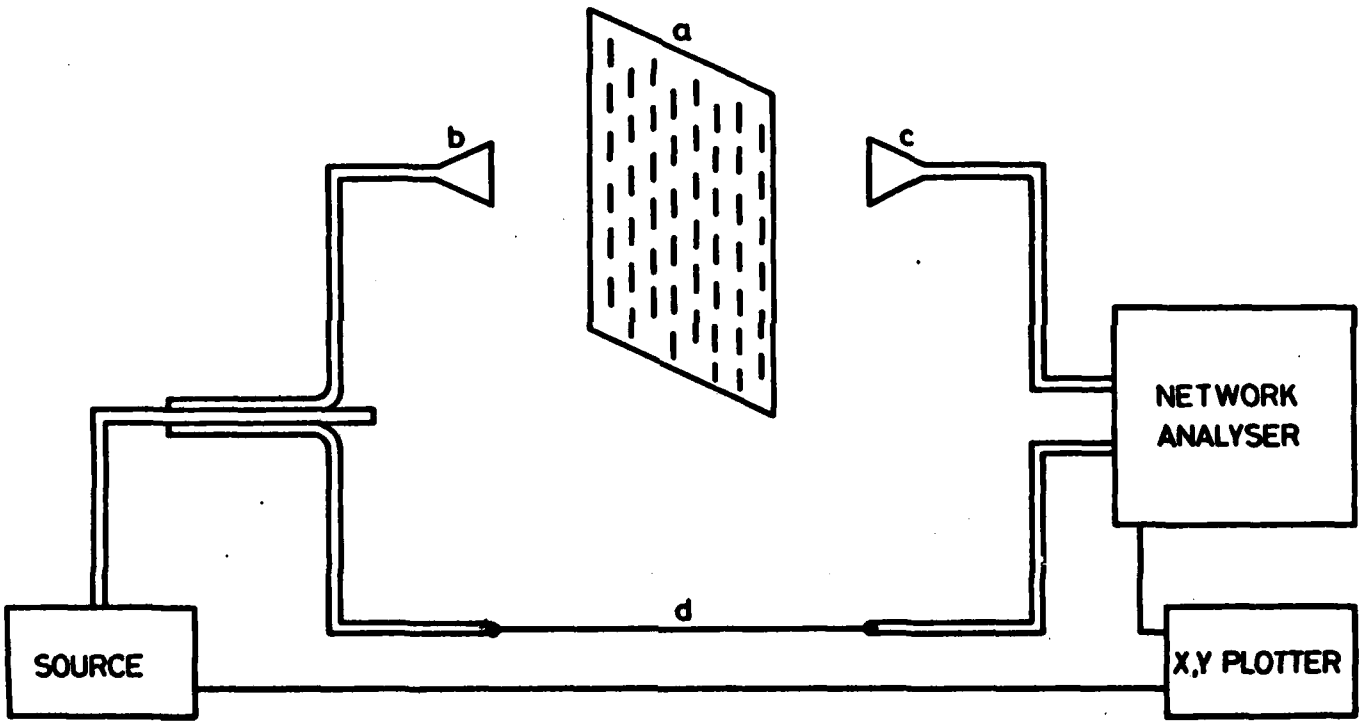

FIG 2

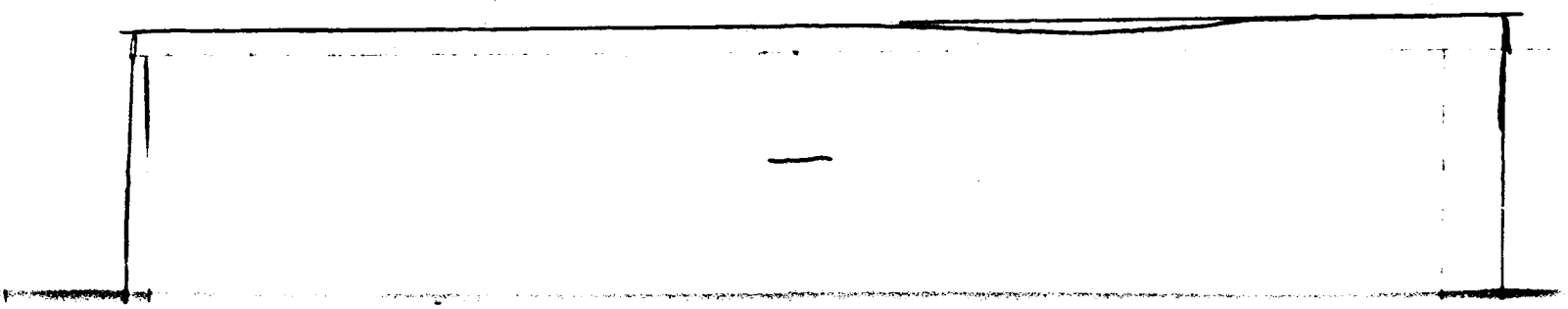

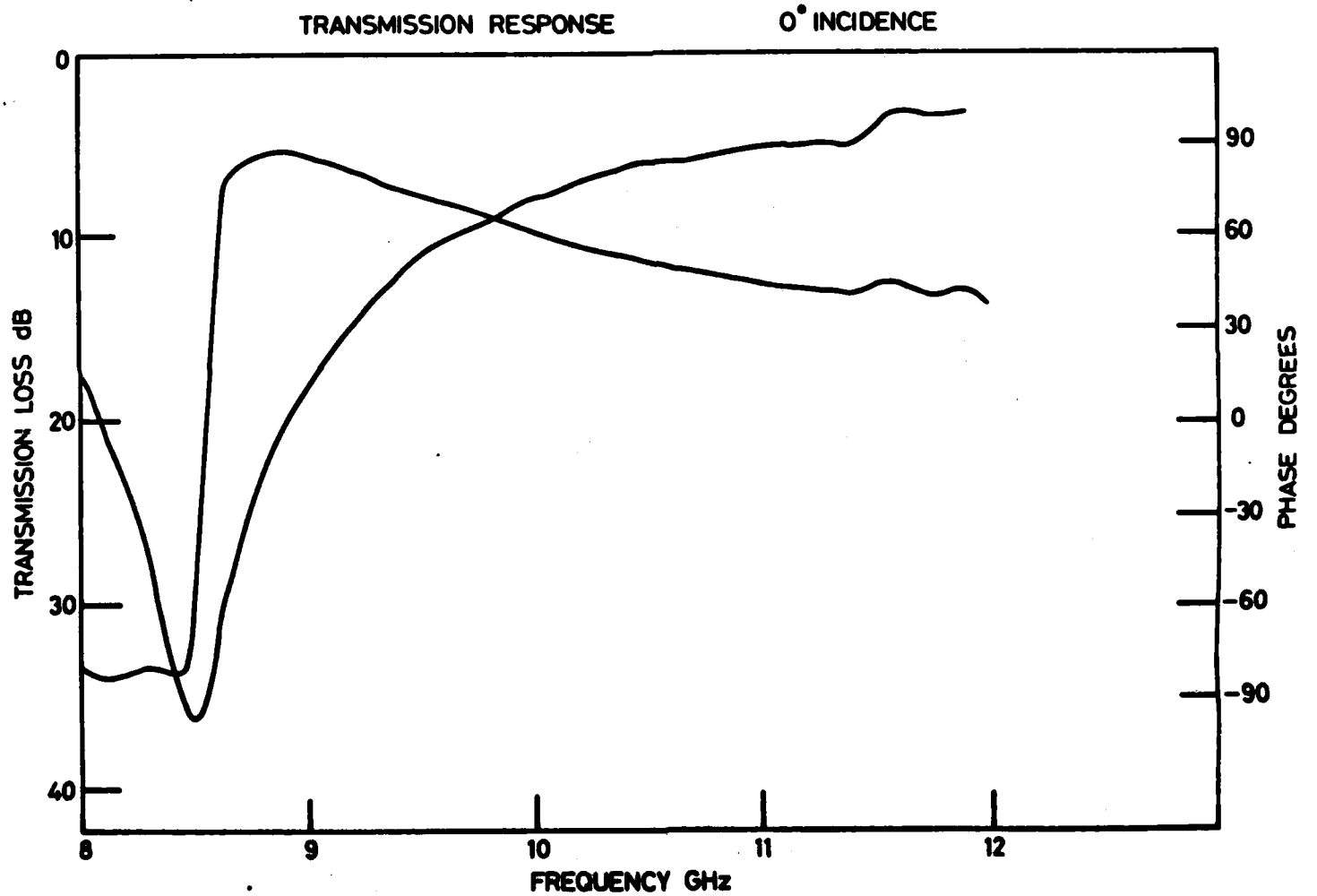
TRANSMISSION RESPONSE
0° INCIDENCE
TRANSMISSION LOSS dB
0
10
20
30
40
PHASE DEGREES
90
60
30
0
-30
-60
-90
8
9
10
11
12
FREQUENCY GHz

FIG 3

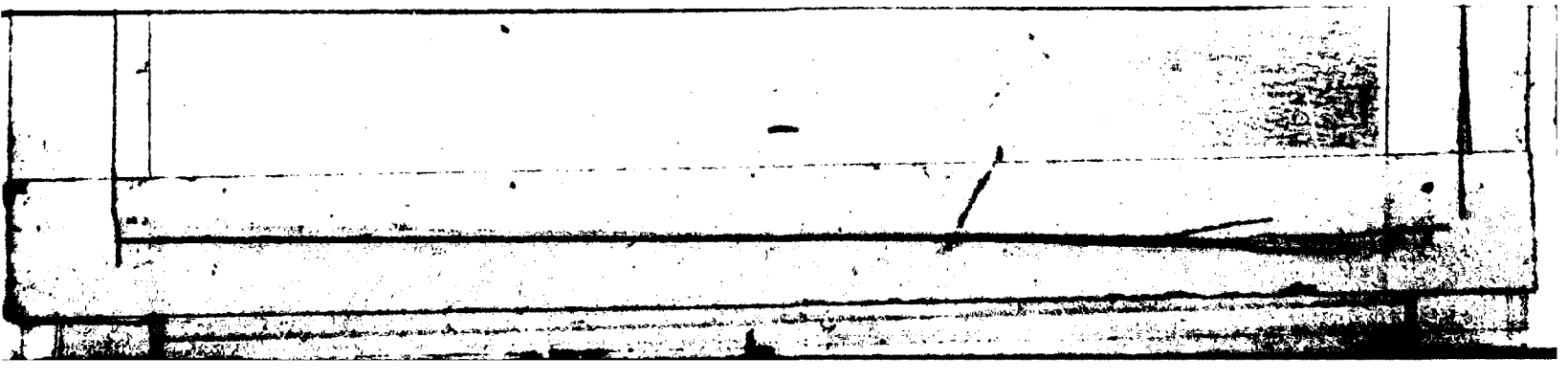

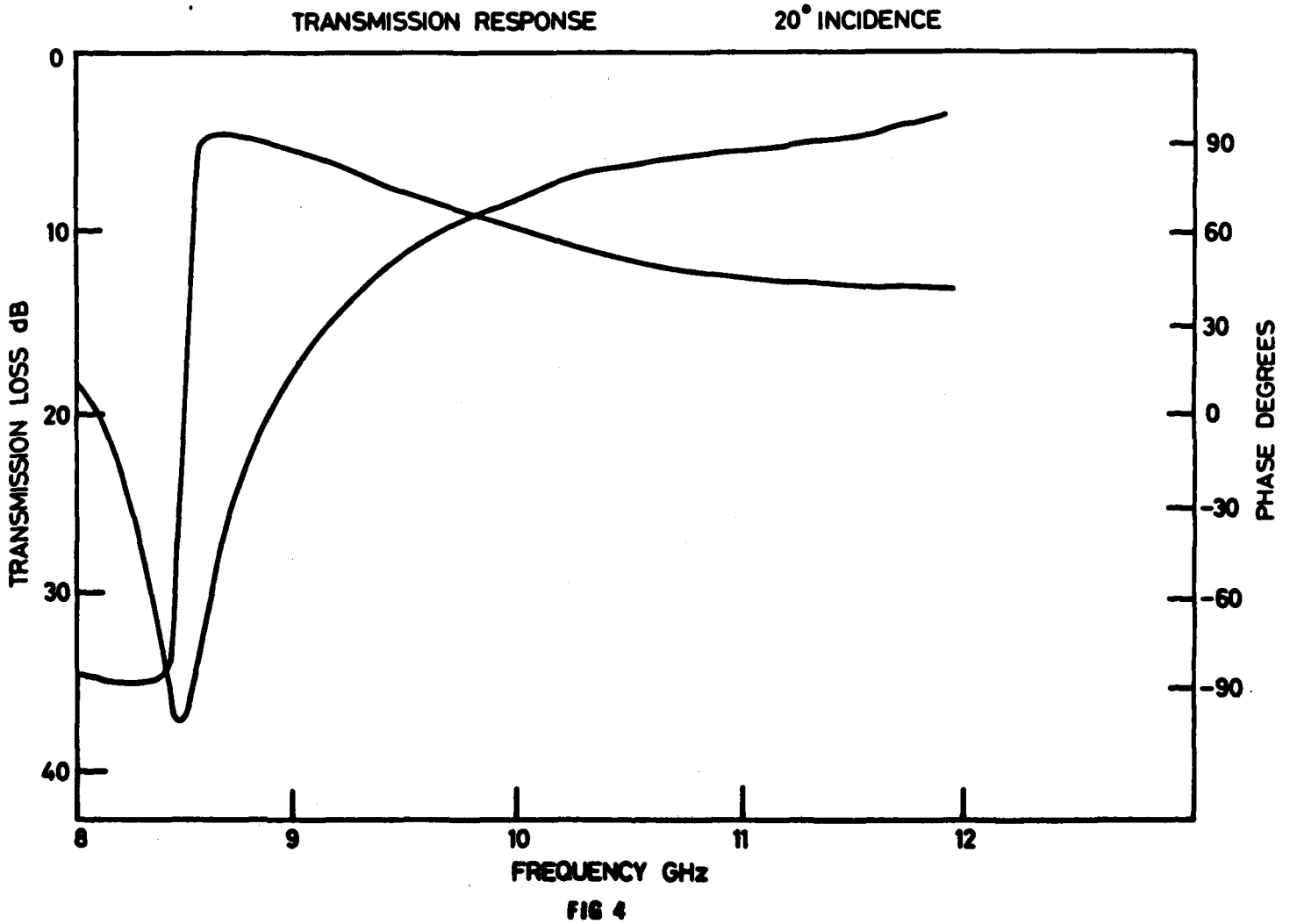
TRANSMISSION RESPONSE
20° INCIDENCE
TRANSMISSION LOSS dB
0
10
20
30
40
PHASE DEGREES
90
60
30
0
-30
-60
-90
8
9
10
11
12
FREQUENCY GHz

FIG 4

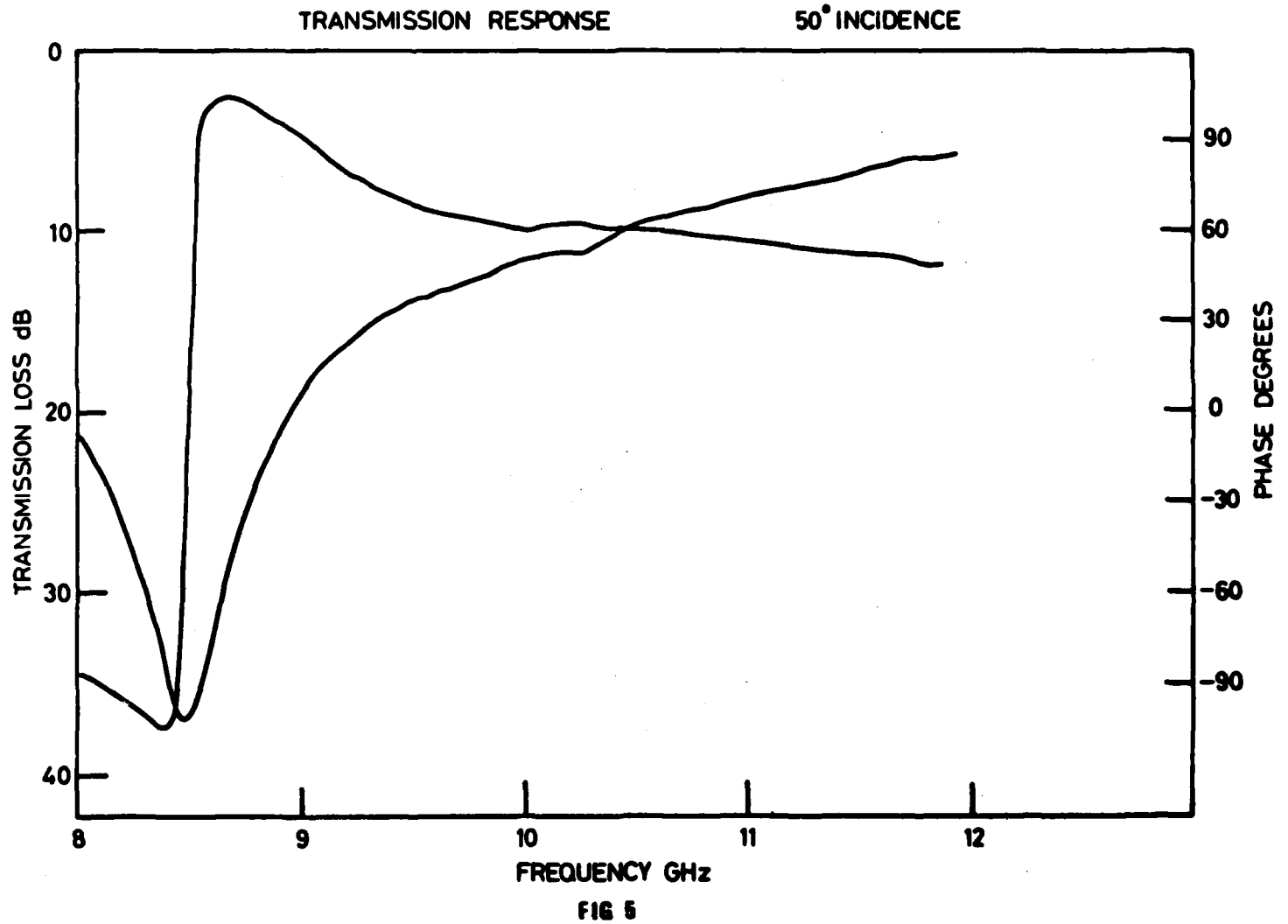
TRANSMISSION RESPONSE
50° INCIDENCE
TRANSMISSION LOSS dB
0
10
20
30
40
PHASE DEGREES
90
60
30
0
-30
-60
-90
8
9
10
11
12
FREQUENCY GHz

FIG 5

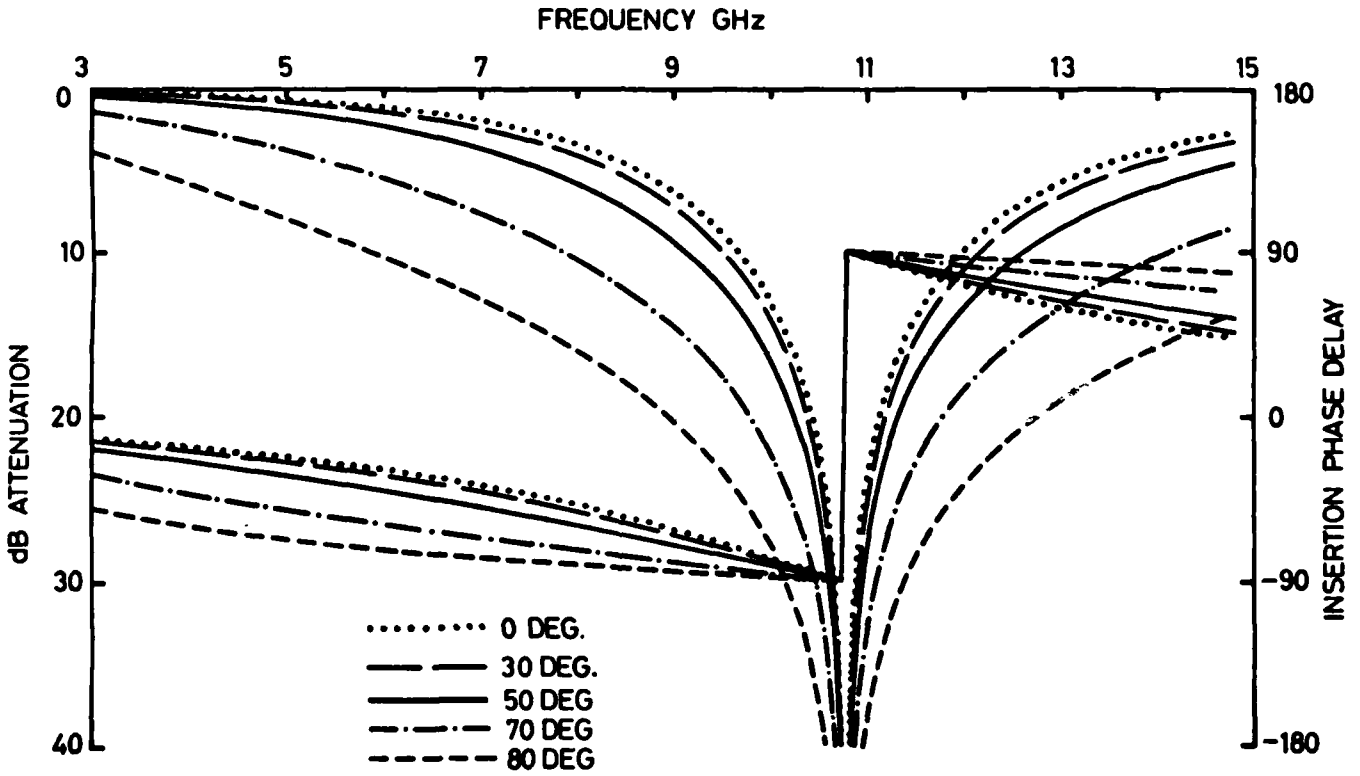
FREQUENCY GHz
3
5
7
9
11
13
15
0
10
20
30
40
dB ATTENUATION
180
90
0
-90
-180
INSERTION PHASE DELAY
0 DEG.
30 DEG.
50 DEG
70 DEG
80 DEG

FIG 6

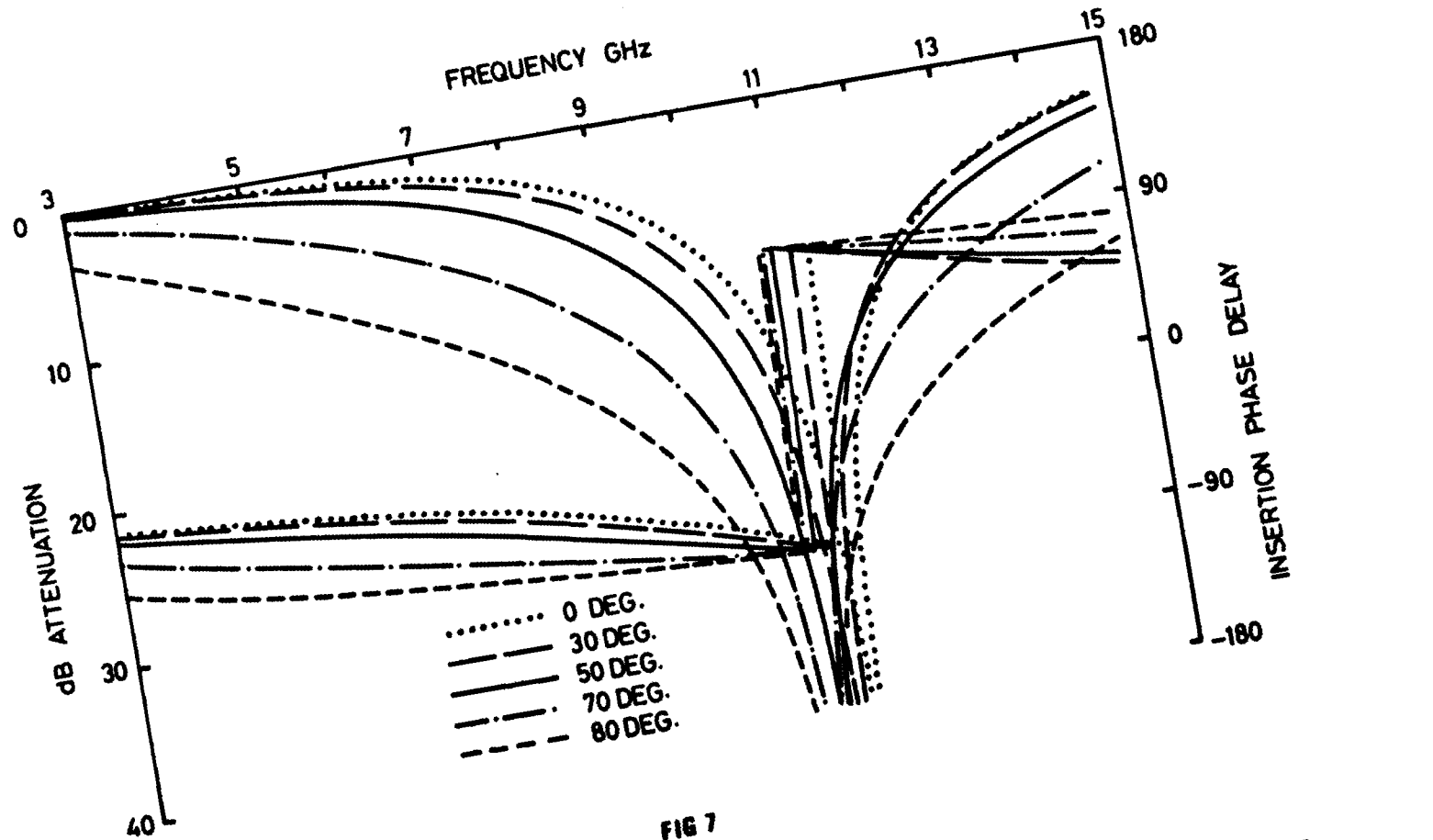
FREQUENCY GHz
3
5
7
9
11
13
15
0
10
20
30
40
dB ATTENUATION
180
90
0
-90
-180
INSERTION PHASE DELAY
0 DEG.
30 DEG.
50 DEG.
70 DEG.
80 DEG.

FIG 7

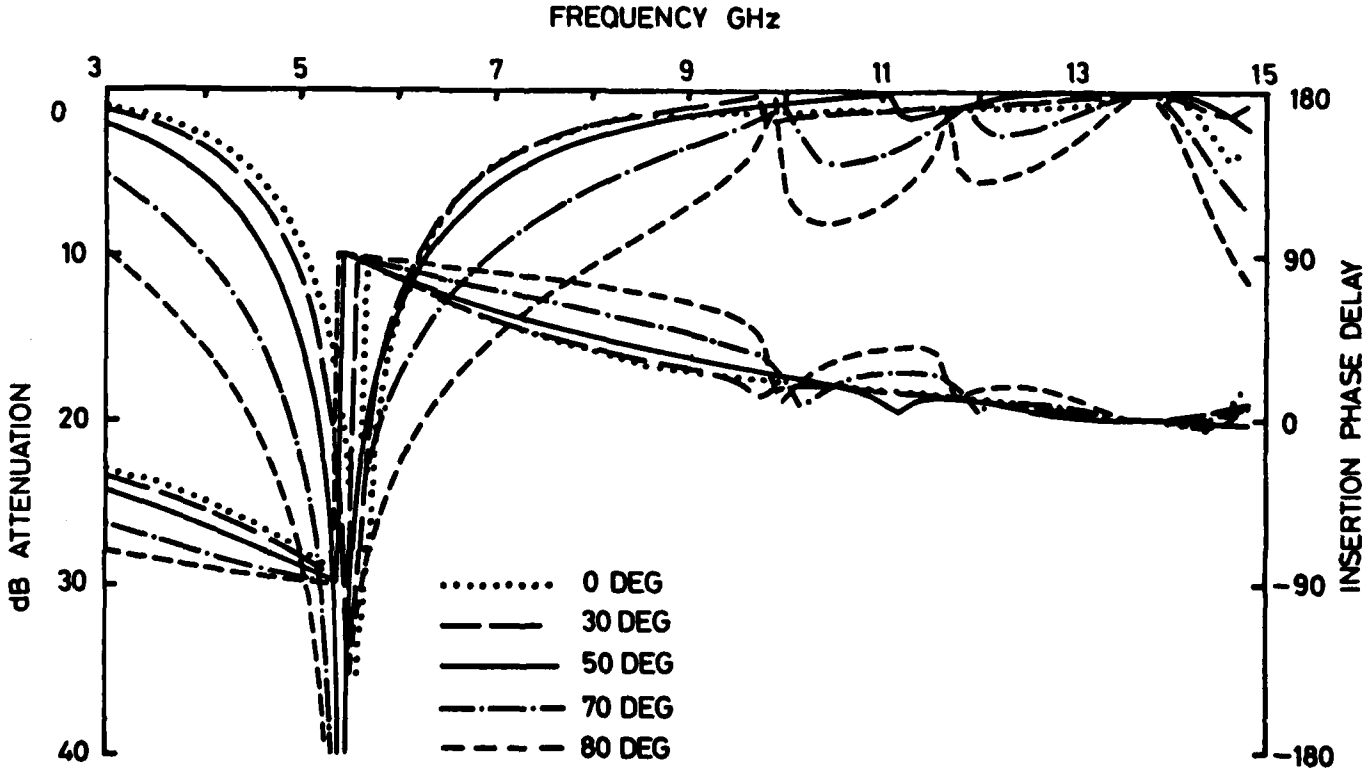
FREQUENCY GHz
3
5
7
9
11
13
15
0
10
20
30
40
dB ATTENUATION
180
90
0
-90
-180
INSERTION PHASE DELAY
0 DEG
30 DEG
50 DEG
70 DEG
80 DEG

FIG 8

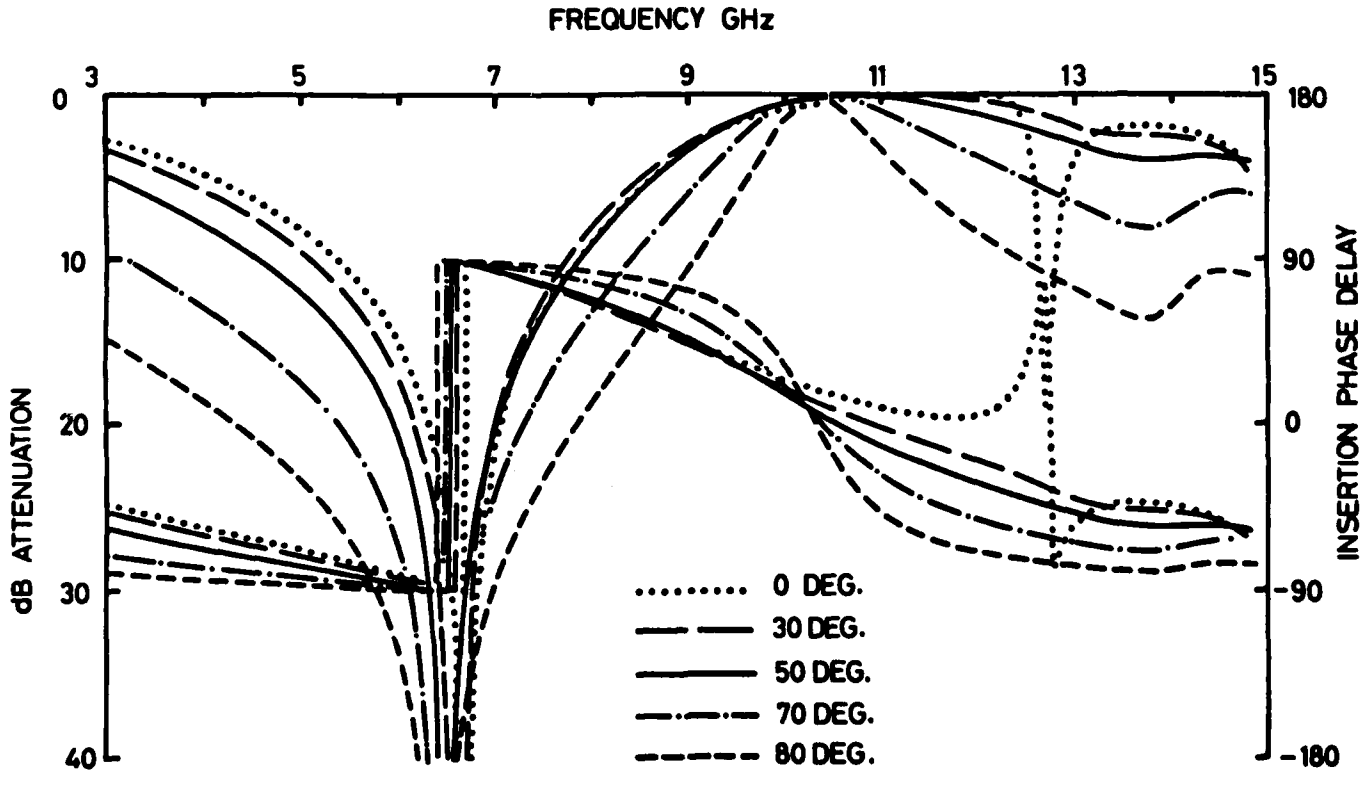
FREQUENCY GHz
3
5
7
9
11
13
15
0
10
20
30
40
dB ATTENUATION
180
90
0
-90
-180
INSERTION PHASE DELAY
0 DEG.
30 DEG.
50 DEG.
70 DEG.
80 DEG.

FIG 9

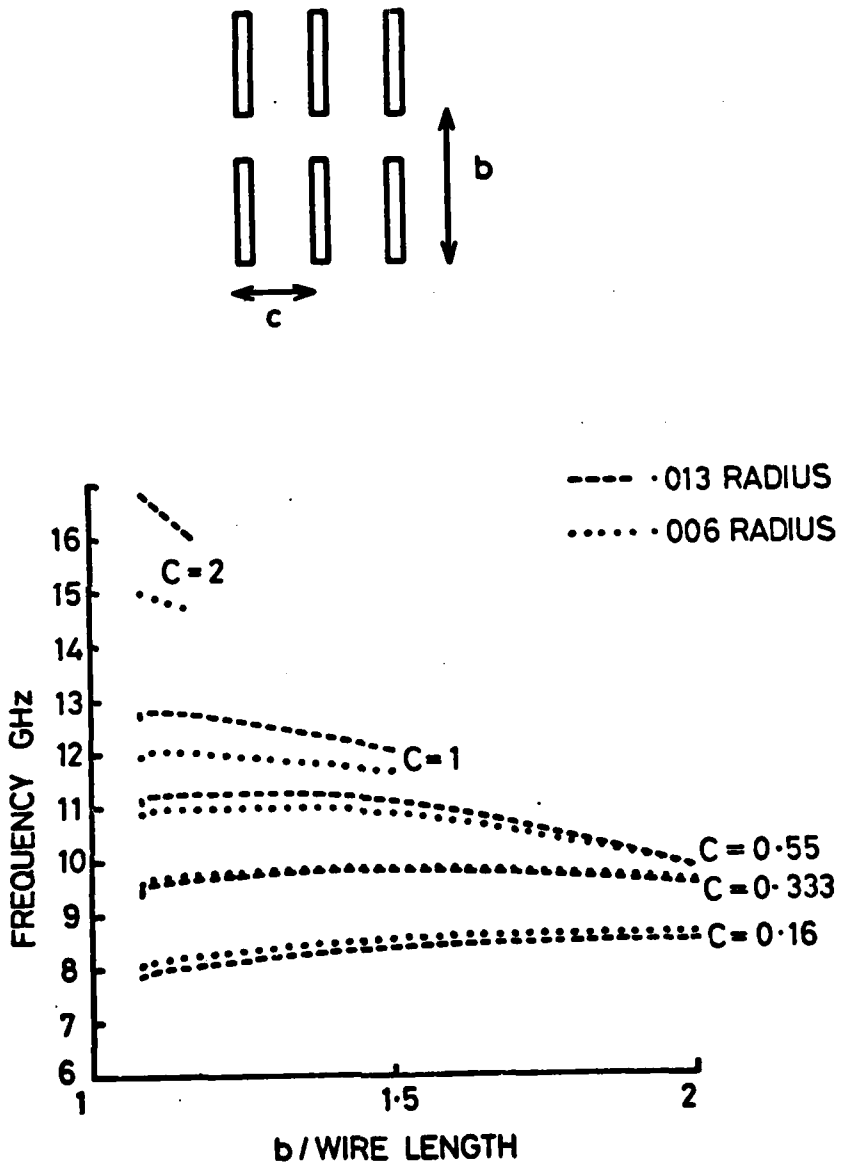
b
c
·013 RADIUS
·006 RADIUS
C = 2
C = 1
C = 0·55
C = 0·333
C = 0·16
FREQUENCY GHz
16
15
14
13
12
11
10
9
8
7
6
1
1·5
2
b / WIRE LENGTH

FIG 10

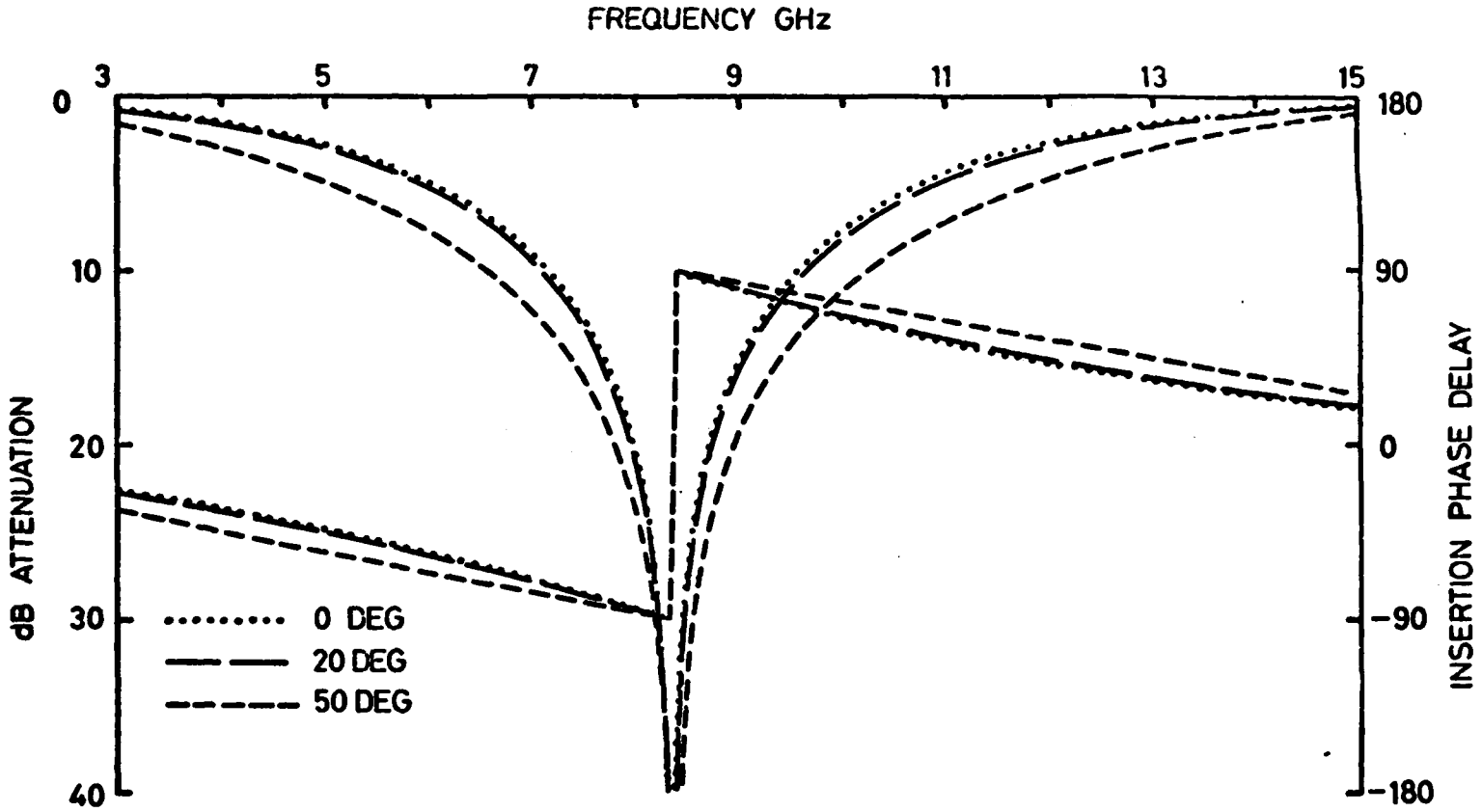
FREQUENCY GHz
3
5
7
9
11
13
15
0
10
20
30
40
dB ATTENUATION
180
90
0
-90
-180
INSERTION PHASE DELAY
0 DEG
20 DEG
50 DEG

FIG 11

DOCUMENT CONTROL SHEET

Overall security classification of sheet ..... UNCLASSIFIED .....

(As far as possible this sheet should contain only unclassified information. If it is necessary to enter classified information, the box concerned must be marked to indicate the classification eg (R) (C) or (S))

1. DRIC Reference (if known)	2. Originator's Reference Memorandum 3618	3. Agency Reference	4. Report Security Classification UNLIMITED Unclassified
5. Originator's Code (if known)	6. Originator (Corporate Author) Name and Location Royal Signals and Radar Establishment		
5a. Sponsoring Agency's Code (if known)	6a. Sponsoring Agency (Contract Authority) Name and Location		

7. Title
A PLANE WAVE EXPANSION SOLUTION FOR THE SCATTERING FROM A FREQUENCY-SELECTIVE SURFACE IN THE PRESENCE OF A DIELECTRIC

7a. Title in Foreign Language (in the case of translations)

7b. *Presented at (for conference papers)* Title, place and date of conference

8. Author 1 Surname, initials	9(a) Author 2	9(b) Authors 3,4...	10. Date	pp. ref.
Gallagher J G	Brammer D J			

11. Contract Number	12. Period	13. Project	14. Other Reference

15. Distribution statement
UNLIMITED

Descriptors (or keywords)

continue on separate piece of paper

Abstract The scattering of a plane wave from a periodic broken-wire grid buried in a dielectric sheet is studied for a general angle of incidence and for arbitrary linear polarisation. The scattered field is expanded in a set of Floquet modes, and the modal coefficients are obtained through the current expansion for a reflecting antenna. The general formulation of the problem is applicable for grids in an infinite dielectric and when located at the boundary interface of two dielectrics. A moment method is used to determine the current on the grid elements and numerical results for the transmission characteristics of several different grid configurations are presented. In addition, the effect on the resonant frequency of parametric variations in the grid geometry is determined. Predicted results are compared with measured transmission characteristics and show excellent agreement.

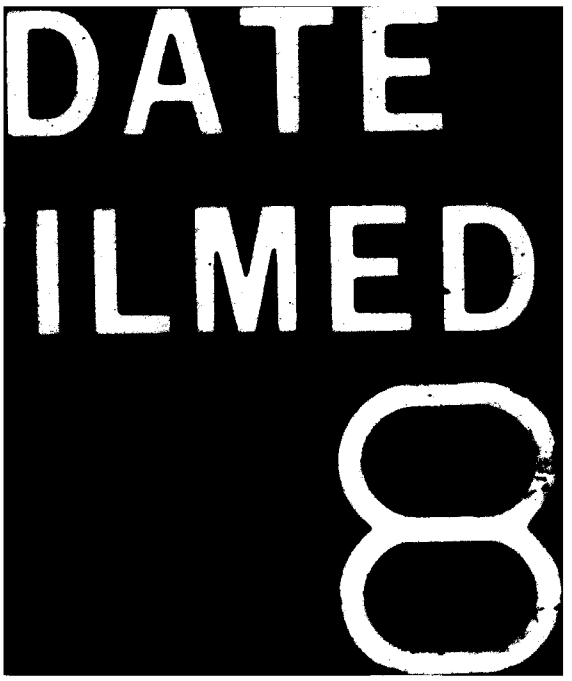
DATE
ILMED
8